12. Clayton, D. D., Dwek, E. & Woosley, S. E. Isotopic anomalies and proton irradiation in the early solar system. *Astrophys. J.* **214,** 300–315 (1977).
13. Heymann, D., Dziczkaniec, M., Walker, A., Huss, G. & Morgan, J. A. Effects of proton irradiation on a gas phase in which condensation take place. I. negative ^{26}Mg anomalies and ^{26}Al. *Astrophys. J.* **225,** 1030–1044 (1978).
14. Lee, T. A local proton irradiation model for isotopic anomalies in the solar system. *Astrophys. J.* **219,** 217–226 (1978).
15. Wasserburg, G. J. & Arnould, M. in *Lecture Notes in Physics 287, 4th Workshop on Nuclear Astrophysics* (eds Hillebrandt, W. *et al.*) 262–276 (Springer, Heidelberg, 1987).
16. Clayton, D. D. & Jin, L. A new interpretation of ^{26}Al in meteoritic inclusions. *Astrophys. J. Lett.* **451,** L87–L91 (1995).
17. Shu, F. H., Shang, H. & Lee, T. Toward an astrophysical theory of chondrites. *Science* **271,** 1545–1552 (1996).
18. Shu, F. H., Shang, H., Glassgold, E. & Lee, T. X-rays and fluctuating X-wind from protostars. *Science* **277,** 1475–1479 (1997).
19. Srinivasan, G., Sahijpal, S., Ulyanov, A. A. & Goswami, J. N. Ion microprobe studies of Efremovka CAIs: II. Potassium isotope composition and ^{41}Ca in the early solar system. *Geochim. Cosmochim. Acta* **60,** 1823–1835 (1996).
20. Goswami, J. N., Srinivasan, G. & Ulyanov, A. A. Ion microprobe studies of Efremovka CAIs: I. Magnesium isotope composition. *Geochim. Cosmochim. Acta* **58,** 431–447 (1994).
21. Fahey, A. J., Goswami, J. N., McKeegan, K. D. & Zinner, E. K. ^{26}Al, ^{244}Pu, ^{50}Ti, REE, and trace element abundances in hibonite grains from CM and CV meteorites. *Geochim. Cosmochim. Acta* **51,** 329–350 (1987).
22. Cantanzaro, E. J., Murphy, T. J., Garner, E. L. & Shields, W. R. Absolute isotopic abundance ratios and atomic weights of magnesium. *J. Res. NBS* **70a,** 453–458 (1966).
23. MacPherson, G. J., Davis, A. M. & Zinner, E. K. The distribution of aluminum-26 in the early solar system—A reappraisal. *Meteoritics* **30,** 365–386 (1995).
24. Garner, E. L., Murphy, T. J., Gramlich, J. W., Paulsen, P. J. & Barnes, I. L. Absolute isotopic abundance ratios and the atomic weight of a reference sample of potassium. *J. Res. NBS* **79a,** 713–725 (1975).
25. Srinivasan, G., Ulyanov, A. A. & Goswami, J. N. ^{41}Ca in the early solar system. *Astrophys. J. Lett.* **431,** L67–L70 (1994).
26. Allen, J. M., Grossman, L., Lee, T. & Wasserburg, G. J. Mineralogy and petrography of HAL, an isotopically-unusual Allende inclusion. *Geochim. Cosmochim. Acta* **44,** 685–699 (1980).
27. Goswami, J. N., Marhas, K. K. & Sahijpal, S. Production of short-lived nuclides by solar energetic particles in the early solar system (Abstr.). *Lunar Planet. Sci.* **XXVIII,** 439–440 (1997).
28. Arnould, M., Meynet, G. & Paulus, G. in *Astrophysical Implications of the Laboratory Study of Presolar Materials* (eds Bernatowicz, T. & Zinner, E.) 179–202 (AIP Press, New York, 1997).
29. Boss, A. P. & Foster, P. N. in *Astrophysical Implications of the Laboratory Study of Presolar Materials* (eds Bernatowicz, T. & Zinner, E.) 649–664 (AIP Press, New York, 1997).
30. Cameron, A. G. W., Vanhala, H. & Hölflich, P. in *Astrophysical Implications of the Laboratory Study of Presolar Materials* (eds Bernatowicz, T. & Zinner, E.) 665–696 (AIP Press, New York, 1997).
31. Cameron, A. G. W. The first ten million years in the solar nebula. *Meteoritics* **30,** 133–161 (1995).

Acknowledgements. We are grateful to G. J. Wasserburg, G. J. MacPherson and A. A. Ulyanov for providing the samples of Allende and Efremovka CAIs for our study. We also thank E. J. Olsen of the Field Museum of Natural History for specimens of Murchison and Allende from which SH-7, BB-4, HAL and the seven hand-picked grains were extracted. We appreciate comments received from A. G. W. Cameron and E. Zinner. We acknowledge support from the Department of Space, Government of India (S.S. and J.N.G.) and from the National Aeronautics and Space Administration (A.M.D., L.G. and R.S.L.). J.N.G. also acknowledges hospitality provided by the Lunar and Planetary Institute, Houston, during the preparation of this manuscript.

Correspondence and requests for materials should be addressed to J. N. Goswami (e-mail: goswami@prl.ernet.in).

Softening of nanocrystalline metals at very small grain sizes

Jakob Schiøtz, Francesco D. Di Tolla* & Karsten W. Jacobsen

Center for Atomic-scale Materials Physics and Department of Physics, Technical University of Denmark, DK2800 Lyngby, Denmark

Nanocrystalline solids, in which the grain size is in the nanometre range, often have technologically interesting properties such as increased hardness and ductility. Nanocrystalline metals can be produced in several ways, among the most common of which are high-pressure compaction of nanometre-sized clusters and high-energy ball-milling[1–4]. The result is a polycrystalline metal with the grains randomly orientated. The hardness and yield stress of the material typically increase with decreasing grain size, a phenomenon known as the Hall–Petch effect[5,6]. Here we present computer simulations of the deformation of nanocrystalline copper, which show a softening with grain size (a reverse Hall–Petch effect[3,7]) for the smallest sizes. Most of the plastic deformation is due to a large number of small 'sliding' events of atomic planes at the grain boundaries, with only a minor part being caused by dislocation activity in the grains; the softening that we see at small grain sizes is therefore due to the larger fraction of atoms at grain boundaries. This softening will ultimately impose a limit on how strong nanocrystalline metals may become.

To simulate the behaviour of nanocrystalline metals with the computer, we construct nanocrystalline 'samples' with structures similar to those observed experimentally: essentially equiaxed dislocation-free grains separated by narrow straight grain boundaries[1]. Each sample contains 8–64 grains in a 10.6-nm cube of material, resulting in grain sizes from 3.3 to 6.6 nm. The grains are produced by a Voronoi construction[8]: a set of grain centres are chosen at random, and the part of space closer to a given centre than to any other centre is filled with atoms in an f.c.c. (face-centred cubic) lattice with a randomly selected crystallographic orientation. A typical 'sample' is shown in Fig. 1a. To mimic the system's being deep within the bulk of a large sample, the system is replicated infinitely in all three spatial directions (periodic boundary conditions). The forces between the atoms are calculated with the effective-medium theory[9,10], which suitably describes many-atom interactions in metals. The metal chosen for these simulations is copper; very similar results were obtained with palladium. Before deforming the system we 'anneal' it by running a 50-ps molecular dynamics simulation at 300 K, allowing unfavourable configurations in the grain boundaries to relax. Doubling the duration of annealing does not have any significant effect, nor does an increase in the temperature to 600 K.

The main part of the simulation is a slow uniaxial deformation while minimizing the energy with respect to all atomic coordinates. The deformation is applied by expanding the simulation cell in one direction, while the size is allowed to relax in the two perpendicular directions.

The initial and final configurations of such a simulation with a total strain of 10% are shown in Fig. 1. We see how the grain boundaries have become thicker, indicating that significant activity has taken place there. In the grains a few stacking faults have appeared. They are the signature of dislocation activity within the grains.

To facilitate the analysis of the simulations, we identify which atoms are located at grain boundaries and which are inside the grains, by determining the local crystalline order[11,12]. Atoms in local f.c.c. order are considered to be 'inside' the grains; atoms in local h.c.p. (hexagonal close-packed) order are classified as stacking faults. All other atoms are considered as belonging to the grain boundaries. Unlike conventional materials, where the volume occupied by the grain boundaries is very small, a significant fraction (30–50%) of the atoms are in the grain boundaries, in agreement with theoretical estimates[2].

As the deformation takes place, we calculate the average stress in the sample as a function of the amount of deformation. For each grain size we simulated the deformation of seven different initial configurations. Figure 2a shows the obtained average deformation curves. We see a linear elastic region with a Young's modulus around 90–105 GPa (increasing with increasing grain size), compared with 124 GPa in macrocrystalline Cu (ref. 13). This is caused by the large fraction of atoms in the grain boundaries having a lower Young's modulus[14,15]. A similar reduction is seen in simulations where the nanocrystalline metal is grown from a molten phase[16]. The elastic region is followed by plastic yielding at around 1 GPa, and finally the plastic deformation saturates at a maximal flow stress around 3 GPa. The theoretical shear stress of a perfect single crystal is approximately 6 GPa for the potential used.

The main deformation mode is illustrated in Fig. 3b, where the relative motions of the atoms is shown. We see that most of the deformation occurs in the grain boundaries in the form of a large number of small sliding events, where only a few atoms (or sometimes a few tens of atoms) move with respect to each other. Occasionally a partial dislocation is nucleated at a grain boundary and moves through a grain. Such events are responsible for a minor part of the total deformation, but in the absence of diffusion they are

* Present address: SISSA, Via Beirut 2-4, I-34014 Grignano (TS), Italy.

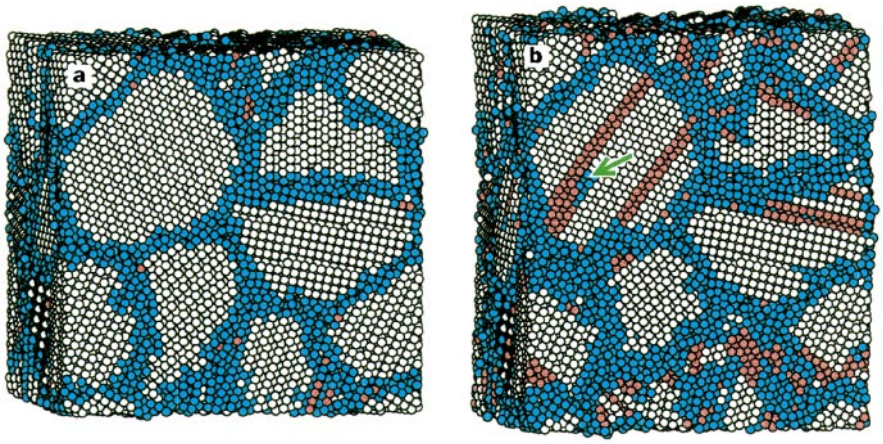

Figure 1 A simulated nanocrystalline copper sample before (**a**) and after (**b**) 10% deformation. The system contains 16 grains and ~100,000 atoms, giving an average grain diameter of 5.2 nm. Atoms in the grain boundaries are coloured blue, atoms at stacking faults are coloured red. We clearly see stacking faults left behind by partial dislocations that have run through the grains during the deformation processes. Such stacking faults would be removed if a second partial dislocation followed the path of the first, but this is not observed in the present simulations. In the left side of the system, a partial dislocation on its way through a grain is seen (green arrow in **b**).

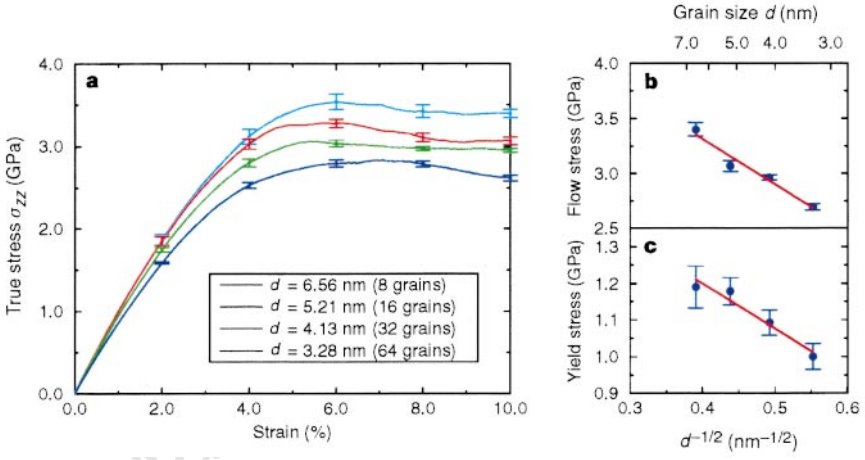

Figure 2 The effect of grain size on deformation. **a**, The average stress in the direction of the stretch (σ_{zz}) versus strain for each grain size. Each curve is the average over seven simulations. The curves show the response of the material to mechanical deformation. In the linear part of the curve (low strains) the deformation is mainly elastic; if the tensile load is removed, the material will return to the original configuration. As the deformation is increased, irreversible plastic deformation becomes important. For large deformations plastic processes relieve the stress, and the curves level off. We see a clear grain-size dependence, which is summarized to the right. **b** and **c**, The maximal flow stress and the yield stress as a function of grain size. The yield stress decreases with decreasing grain size, resulting in a reverse Hall–Petch effect. (The maximal flow stress is the stress at the flat part of the stress–strain curves; the yield stress is defined as the stress where the strain departs 0.2% from linearity.)

required to allow for deformations of the grains, as they slide past each other. No dislocation motion is seen in Fig. 3, as none occurred at that time of the simulation. As the grain size is reduced a larger fraction of the atoms belongs to the grain boundaries, and grain-boundary sliding becomes easier. This leads to a softening of the material as the grain size is reduced (Fig. 2).

The observed deformation mode is in some ways similar to the manner in which grain boundaries carry most of the deformation in superplastic deformation[17,18]. This is consistent with recent simulations of flow speed in nanocrystalline metals[25]. However, in superplasticity the grain-boundary sliding is thermally activated, whereas here it occurs at zero temperature driven by the high stress.

In conventional metals an increase in hardness and yield strength with decreasing grain size is observed. This is called the Hall–Petch effect, and is generally considered to be caused by the grain boundaries, impeding the generation and/or motion of dislocations as the grains get smaller; this behaviour extends far into the nanocrystalline regime[3,19]. The grain sizes in the present simulations correspond to the smallest grain sizes that can be obtained experimentally. In that regime the Hall–Petch effect is often seen to cease or even to reverse, but the results depend strongly on the sample history and on the method used to vary the grain size. Many mechanisms have been proposed for this reverse Hall–Petch effect: increased porosity at small grain sizes[3], suppression of dislocation pile-ups[20], dislocation motion through multiple grains[21], sliding in the grain boundaries[22], and enhanced diffusional creep in the grain boundaries[7]. Direct measurements of the creep rates seem to rule out the last mechanism[19,20], but otherwise no consensus has been reached. The present simulations indicate that the behaviour characteristic of a reverse Hall–Petch effect is possible even in the absence of porosity, and that it may be caused by sliding in the grain boundaries even in the absence of thermally activated processes. We cannot, however, see a cross-over from this 'reverse' behaviour to the normal Hall–Petch regime at larger grain sizes in our simulations, because they become too computationally expensive at these larger sizes. For the same reason, we cannot provide a direct comparison with the behaviour of the bulk metal.

A direct quantitative comparison between the simulations and the experimental results should be done with caution. The main difference between the simulated strain–stress curves and experimental curves is the level of the yield stress, which is approximately twice what is observed in experiments on low-porosity samples (400 MPa)[23]. This value is, however, obtained for a grain size of around 40 nm; extrapolation to 7-nm grains gives a yield strength around 800 MPa (ref. 23), assuming that the Hall–Petch behaviour persists to these grain sizes. Experimentally produced nanocrystalline samples typically contain voids and surface defects, reducing the strength of the material. Surface defects alone have been shown

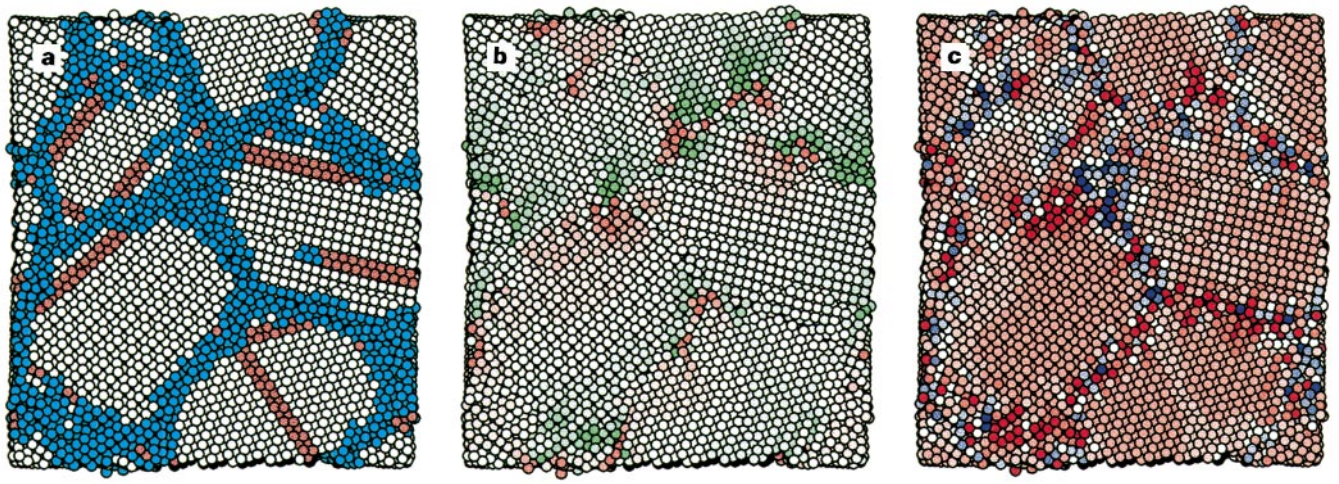

Figure 3 Snapshot of grain structure, displacements and stresses at 8% deformation. **a**, The position of the grain boundaries (blue) and stacking faults (red) at this point in the simulation. **b**, The relative motion of the atoms in the *z* direction (up, in the plane of the paper) during the preceding 0.4% deformation. The green atoms move up, red atoms move down. We see many small, independent slip events in the grain boundaries; this is the main deformation mode. **c**, The stress field (the σ_{33} component) in the grains. Shades of red indicate tensile stress, shades of blue compressive stress (dark colours correspond to high stresses). The stress in the grain boundaries is seen to vary considerably on the atomic scale, and the average stress is ~10–20% lower than in the grains.

to be able to reduce the strength of nanocrystalline palladium by at least a factor of five[19,24].

Another difference is the absence of thermally activated processes in the simulations. These processes give rise to a strain-rate dependence of the mechanical properties, leading to higher yield stresses at higher strain rates where there is less time available for the activated processes to occur. Thermally activated processes are not included in the simulations because the energy minimization procedure quickly removes all thermal energy. No timescale or strain rate can be directly defined in the simulations, but in a sense the procedure corresponds to a slow strain at very low temperatures: thermally activated processes are excluded but the energy created by the work is carried away fast. The above-mentioned creep measurements[19,20] indicate that diffusion does not play a major role during deformation.

During the later part of the simulated deformation larger average stresses build up within the grains than in the grain boundaries (10–20%), and larger stresses build up in the larger grains (see Fig. 3c). This results in a larger variation in the maximal flow stress than in the yield stress (Fig. 2b): when the grain size is increased the maximal flow stress increases, both because the stresses in the grains increase and because the number of atoms within the grains becomes a larger fraction of the total number of atoms. □

Received 23 June; accepted 29 October 1997.

1. Siegel, R. W. in *Encyclopedia of Applied Physics* Vol. 11, 173–199 (VCH, New York, 1994).
2. Siegel, R. W. What do we really know about the atomic-scale structure of nanophase materials? *J. Phys. Chem. Solids* **55,** 1097–1106 (1994).
3. Siegel, R. W. & Fougere, G. E. in *Nanophase Materials: Synthesis—Properties—Applications* (eds Hadjipanayis, G. C. & Siegel, R. W.) 233–261 (NATO-ASI Ser. E, Vol. 260, Kluwer, Dordrecht, 1994).
4. Gleiter, H. in *Mechanical Properties and Deformation Behavior of Materials Having Ultra-Fine Microstructures* (ed. Nastasi, M.) 3–35 (Kluwer, Dordrecht, 1993).
5. Hall, E. O. The deformation and ageing of mild steel: III Discussion of results. *Proc. Phys. Soc. Lond. B* **64,** 747–753 (1951).
6. Petch, N. J. The cleavage of polycrystals. *J. Iron Steel Inst.* **174,** 25–28 (1953).
7. Chokshi, A. H., Rosen, A., Karch, J. & Gleiter, H. On the validity of the Hall–Petch relationship in nanocrystalline materials. *Scripta Metall.* **23,** 1679–1684 (1989).
8. Voronoi, G. *Z. Reine Angew. Math.* **134,** 199 (1908).
9. Jacobsen, K. W., Nørskov, J. K. & Puska, M. J. Interatomic interactions in the effective-medium theory. *Phys. Rev. B* **35,** 7423–7442 (1987).
10. Jacobsen, K. W., Stoltze, P. & Nørskov, J. K. A semi-empirical effective medium theory for metals and alloys. *Surf. Sci.* **366,** 394–402 (1996).
11. Jónsson, H. & Andersen, H. C. Icosahedral ordering in the Lennard–Jones liquid and glass. *Phys. Rev. Lett.* **60,** 2295–2298 (1988).
12. Clarke, A. S. & Jónsson, H. Structural changes accompanying densification of random-sphere packings. *Phys. Rev. E* **47,** 3975–3984 (1993).
13. Gschneidner, K. A. Physical properties and interrelationships of metallic and semimetallic elements. *Solid State Phys.* **16,** 275–426 (1964).
14. Shen, T. D., Koch, C. C., Tsui, T. Y. & Pharr, G. M. On the elastic moduli of nanocrystalline Fe, Cu, Ni, and Cu-Ni alloys prepared by mechanical milling/alloying. *J. Mater. Res.* **10,** 2892–2896 (1995).
15. Kluge, M. D., Wolf, D., Lutsko, J. F. & Phillpot, S. R. Formalism for the calculation of local elastic constants at grain boundaries by means of atomistic simulation. *J. Appl. Phys.* **67,** 2370–2379 (1990).
16. Phillpot, S. R., Wolf, D. & Gleiter, H. Molecular-dynamics study of the synthesis and characterization of a fully dense, three-dimensional nanocrystalline material. *J. Appl. Phys.* **78,** 847–860 (1995).
17. Chokshi, A. H., Mukherjee, A. K. & Langdon, T. G. Superplasticity in advanced materials. *Mater. Sci. Eng. R* **10,** 237–274 (1993).
18. Ridley, N. (ed.) *Superplasticity: 60 years after Pearson* (Institute of Metals, London, 1995).
19. Nieman, G. W., Weertman, J. R. & Siegel, R. W. Mechanical behavior of nanocrystalline Cu and Pd. *J. Mater. Res.* **6,** 1012–1027 (1991).
20. Nieh, T. G. & Wadsworth, J. Hall–Petch relation in nanocrystalline solids. *Scripta Met. Mater.* **25,** 955–958 (1991).
21. Lian, J., Baudelet, B. & Nazarov, A. A. Model for the prediction of the mechanical behaviour of nanocrystalline materials. *Mater. Sci. Eng. A* **172,** 23–29 (1993).
22. Langdon, T. G. The significance of grain boundaries in the flow of polycrystalline materials. *Mater. Sci. Forum* **189–190** 31–42 (1995).
23. Suryanarayanan, R. *et al.* Mechanical properties of nanocrystalline copper produced by solution-phase synthesis. *J. Mater. Res.* **11,** 439–448 (1996).
24. Weertman, J. R. Hall–Petch strengthening in nanocrystalline metals. *Mater. Sci. Eng. A* **166,** 161–167 (1993).
25. Van Swygenhoven, H. & Caro, A. Plastic behavior of nanophase Ni: A molecular dynamics computer simulation. *Appl. Phys. Lett.* **71,** 1652–1654 (1997).

Acknowledgements. We thank J. K. Nørskov, T. Leffers, O. B. Pedersen, A. E. Carlsson and J. P. Sethna for discussions. The Center for Atomic-scale Materials Physics is sponsored by the Danish National Research Foundation.

Correspondence and requests for materials should be addressed to J.S. (e-mail: schiotz@fysik.dtu.dk).

Compound refractive optics for the imaging and focusing of low-energy neutrons

M. R. Eskildsen*, P. L. Gammel†, E. D. Isaacs†, C. Detlefs‡, K. Mortensen* & D. J. Bishop†

** Risø National Laboratory, PO Box 49, DK-4000 Roskilde, Denmark*
† Bell Laboratories, Lucent Technologies, 700 Mountain Avenue, Murray Hill, New Jersey 07974, USA
‡ Ames Laboratory and Department of Physics and Astronomy, Iowa State University, Ames, Iowa 50011, USA

Low-energy neutrons are essential for the analysis and characterization of materials and magnetic structures. However, both continuous (reactor-based) and pulsed (spallation-based) sources of such neutrons suffer from low fluence. Steering and lensing devices could improve this situation dramatically, so increasing spatial resolution, detectable sample volume limits and even perhaps opening the way for the construction of a neutron